Effect of modified Blalock-Taussig shunt anastomosis angle and pulmonary artery diameter on pulmonary flow

Ahmet Arnaz, *Şenol Pişkin[1,2],* *Gökçe Nur Oğuz[1],* *Yusuf Yalçınbaş[3],* *Kerem Pekkan[1],* *Tayyar Sarıoğlu*

Department of Cardiovascular Surgery, Faculty of Medicine, Acıbadem Mehmet Ali Aydınlar University; İstanbul-*Turkey*
[1]Department of Mechanical Engineering, Koç University; İstanbul-*Turkey*
[2]Department of Mechanical Engineering, University of Texas at San Antonio; San Antonio, TX-*USA*
[3]Department of Cardiovascular Surgery, Acıbadem Bakırköy Hospital; İstanbul-*Turkey*

Abstract

Objective: This study aimed to identify the best graft-to-pulmonary artery (PA) anastomosis angle measuring pulmonary blood flow, wall shear stress (WSS), and shunt flow.
Methods: A tetralogy of Fallot with pulmonary atresia computer model was used to study three different modified Blalock-Taussig shunt (mBTS) anastomosis angle configurations with three different PA diameter configurations. Velocity and WSS were analyzed, and the flow rates at the right PA (RPA) and left PA (LPA) were calculated.
Results: A 4-mm and 8-mm diameter of RPA and LPA, respectively with vertical shunt angle produces the highest total flow. In the RPA larger diameter than the LPA configutations, the left-leaning shunt produces the lowest total PA flow whereas in the LPA larger diameter than the RPA configuratios, the right-leaning shunt produces the lowest total PA flow. Therefore, the shunt anastomosis should not be leaned through the narrow side of PA to reach best flow. As the flow inside the shunt increased, WSS also increased due to enhanced velocity gradients.
Conclusion: The anastomosis angle between the conduit and PA affects the flow to PA. Vertical anastomosis configurations increase the total PA flow; thus, these configurations are preferable than the leaned configurations. *(Anatol J Cardiol 2018; 20: 2-8)*
Keywords: modified Blalock-Taussig shunt, shunt stenosis, computational fluid dynamics, hemodynamic, simulations

Introduction

Systemic-to-pulmonary artery (PA) shunts are palliative procedures performed in patients with severe cyanotic congenital heart disease (CCHD) that is associated with decreased or absent pulmonary blood flow. Shunts are used as staging procedures to increase the pulmonary blood flow, improve tissue oxygenation, and promote the normal development of PAs before further palliative or definitive reconstruction (1).

The Blalock-Taussig shunt (BTS) procedure (a subclavian-to-PA shunt) was first described as a systemic-to-pulmonary shunt model in 1945 (2). Later, various in-life modifications to systemic-to-pulmonary shunts were described. However, the modified BTS (mBTS) developed and has been the most favored method since its initial use in 1981 (3). Connecting PA to the systemic circulation (subclavian artery) via a conduit increases the blood flow through PA. Although this method achieved an increased success rate compared with previous methods, it is still associated with high morbidity and mortality (4).

Many studies have highlighted the risk of graft thrombosis and overflow with respect to patients' age and weight and graft diameter. One of the most important complications with mBTS is shunt occlusion, which requires emergency intervention. It can develop gradually or suddenly and causes decreased pulmonary blood flow and decreased O2 saturation, which results in hypoxia and becomes life-threatening (5).

In the current study, we created a CCHD model [tetralogy of Fallot (ToF) with pulmonary atresia] and studied nine different con-

This manuscript was presented in surgery category as "Poster Presentation" at the 7th World Congress of Pediatric Cardiology and Cardiac Surgery (WCPCCS) on July 16-21, 2017, in the Centre Convencions Internacional de Barcelona (CCIB), Barcelona, Spain.
Address for correspondence: Dr. Ahmet Arnaz, Acıbadem Mehmet Ali Aydınlar Üniversitesi Tıp Fakültesi, Kalp ve Damar Cerrahisi Anabilim Dalı, Halit Ziya Uşaklıgil Caddesi No:1, 34140, İstanbul-*Türkiye*
Phone: +90 212 414 45 16 Fax: +90 212 414 44 90 E-mail: ahmetarnaz@yahoo.com
Accepted Date: 13.04.2018 **Available Online Date:** 18.06.2018

DOI:10.14744/AnatolJCardiol.2018.54810

figurations at the PA connection point, accounting for the three possible different shunt angles and three different PA diameters.

Methods

3D geometry and configurations

A virtual computer simulation was used to determine the configuration that achieved the best pulmonary blood flow (Fig. 1). The 3D geometry used in this study included the thoracic aorta, PA, and neck and cerebral arteries. PAs were illustrated based on ToF with pulmonary atresia. The main PA was cut from the ToF template to simulate pulmonary atresia. Changes in shunt geometry were sketched using our in-house anatomical editing software Sketchcad and merged with Geomagic software (Geomagic Inc., NC, USA) (6).

A myriad of variables can be changed in these analyses, and so, the variation in inputs can be quite formidable: systemic and pulmonary anatomy and size, shunt size and length, angulation, systemic vascular resistance (SVR), pulmonary vascular resistance (PVR), "physiological" flows, existence of patent ductus arteriosus (PDA) and major aortapulmonary collateral arteries (MAPCAs), and many more. In this study, the main modifiable factor was the angle of shunt insertion at the PA level; when combined three different pulmonary anastomosis angle with three different PA sizes, this resulted in nine geometrical configurations to be analyzed.

There are three conduits for PA anastomosis: the angle configurations that direct blood flow from the right subclavian artery to the right PA (RPA) and ultimately the left PA (LPA). The first conduit configuration was a straight shunt between two arteries. The other conduits diverged orthogonally from the right subclavian artery and converged to RPA with anastomosis angles of 60° and 120°. All the conduits had an inside diameter of 4 mm.

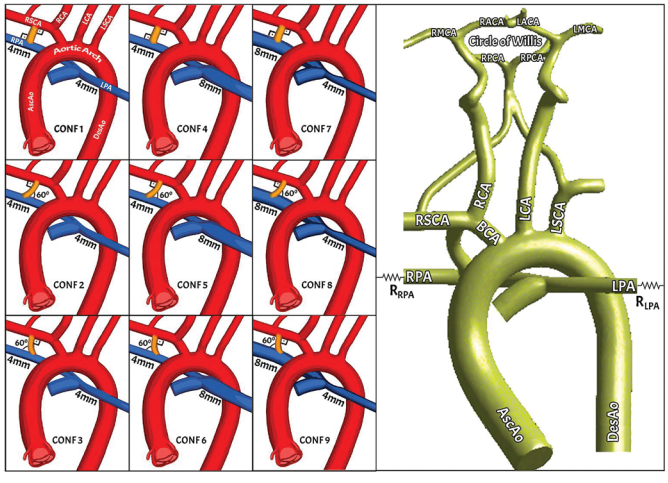

Figure 1. A realistic anatomical model of the thoracic aorta, PAs, and neck and cerebral arteries is reconstructed based on the patient data. The surgical shunt configurations sketched below are applied to this model.
PAs - pulmonary arteries

Table 1. Dimensions of arterial geometry and shunt

Artery	Lumen diameter (mm)
Ascending aorta	10
Arcus aorta	9
Descending aorta	8
Right and left subclavian artery	5
Right and left common carotid artery	4
PTFE conduit	4

Three different PA diameter configurations were produced for all the conduit angle types. In the first configuration, both RPA and LPA had a diameter of 4 mm. In the second configuration, the diameters of RPA and LPA were 8 and 4 mm, respectively. Finally, the third configuration had the opposite diameters (i.e., 4 and 8 mm for RPA and LPA, respectively). These three conduit angles and pulmonary sizes produced nine different configurations in total. The dimensions of the arterial geometry and shunt are shown in Table 1.

Furthermore, six additional cases were designed by separately changing the right and left pulmonary resistance values. The change was limited by 20% increase and decrease compared with the base case having vertical shunt anastomosis (i.e. configuration 1 as shown in Fig. 1-CNF).

Boundary conditions and computational fluid dynamics solver

Based on the typical flow rates observed clinically, all shunt configurations were simulated with an inlet velocity boundary condition at the ascending aorta with a flow rate of 0.0955 kg/s (7). The plug-flow velocity profile was applied in compliance with the standard practice of aortic simulations. Resistance boundary conditions were imposed at each outlet of the aortic arch and pulmonary, neck, and cerebral arteries to represent the downstream systemic vasculature. The resistance values for the artery outlets were calculated in our previous studies by matching the physiological flow distributions (7). These values were slightly adjusted, as reported in our previous study (8), to match the physiological pulmonary-to-systemic flow ratio (Qp/Qs). The resistance value for each cerebral artery was assumed to be the same: 7.968 MPa.s.m^{-3} for the right and left anterior cerebral arteries, right and left middle cerebral arteries, and right and left posterior cerebral arteries. Simulations were run under the same inlet and boundary conditions for all configurations. This allowed us to make comparisons between the conduit anastomosis angle and PA size.

A commercial computational fluid dynamics (CFD) solver FLUENT 15.0 (Ansys, Inc., PA, USA) was used for this study. The CFD code was configured to implement a multigrid artificial compressibility solver for incompressible steady-state Newtonian flows and employed a second-order accurate numerical discretization scheme (7). Steady-state simulations can particularly

Anatol J Cardiol 2018; 20: 2-8
DOI:10.14744/AnatolJCardiol.2018.54810

accurately predict the flow splits and thus can be accepted as an effective methodology.

In this study, there was only one geometry (patient data), and all simulations were performed on this geometry by making necessary shunt and RPA and LPA size configurations and using pulmonary resistance values. Since there were no other geometry data for performing other simulations, statistical analysis results were compared with each other. Besides statistical analysis, mesh sensitivity analysis, which is a standard method for most computational studies, was performed on the basis of a single configuration by changing the mesh element size from coarsest to finest mesh. This size was decreased until the difference of velocity profile between last two consecutive cases was less than 5%. This is less than the typical standard deviation of the other first-stage shunt configurations (8, 9).

For a typical high-density spatial grid with a total of ~1M fluid nodes, a simulation time-step size of 10^{-5} in physical time is required with a grid spacing of 0.6 mm to achieve convergence. The simulations are run until convergence of fluid parameters (i.e. velocity and contunity) up to an accuracy of 10^{-6}. Mass conservation was ensured in all cases having a maximum 10^{-9} L/min difference between the inlet and outlet (7).

Details of the model, solver, and boundary conditions have been presented in our previous publications (7, 8). Thus, only a brief explanation has been provided here.

Calculation of blood damage

The blood damage caused by shear strain due to fluid flow is calculated based on the following equation (9):

$$\frac{\Delta Hb}{Hb}=3.62\times10^{-5}\times\sigma_v^{2.416}\Delta t^{0.785}$$

Where σv is the stress at which the cell is exposed, Δt the total residence time of the blood, ΔHb/Hb the ratio of plasma-free hemoglobin to total hemoglobin. σv was calculated based on the following von Mises equivalent formula:

$$\sigma v=\sqrt{3J_2}$$

$$=\sqrt{\frac{(\sigma_{11}-\sigma_{22})^2+(\sigma_{22}-\sigma_{33})^2+(\sigma_{33}-\sigma_{11})^2+6(\sigma_{12}^2+\sigma_{23}^2+\sigma_{31}^2)}{2}}$$

$$=\sqrt{\frac{(\sigma_1-\sigma_2)^2+(\sigma_2-\sigma_3)^2+(\sigma_3-\sigma_1)^2}{2}}$$

$$=\sqrt{\frac{3}{2}\ S_{ij}S_{ij}}$$

Results

Flow splits

Table 2 summarizes the flow rates at LPA and RPA for all shunt and diameter configurations studied; Figure 2 presents the velocity magnitude colored streamlines.

Table 2. Pulmonary flow rates (10^{-4} kg/s) for RPA-LPA in all cases studied

	Vertical (90°)	Lean right (60°)	Lean left (60°)
RPA:4 mm	173	171	156
LPA:4 mm	122	127	149
Total	295	298	305
RPA:4 mm	172	166	151
LPA:8 mm	165	132	168
Total	337	298	319
RPA:8 mm	182	172	162
LPA:4 mm	146	142	141
Total	329	314	303

RPA - right pulmonary artery; LPA - left pulmonary artery

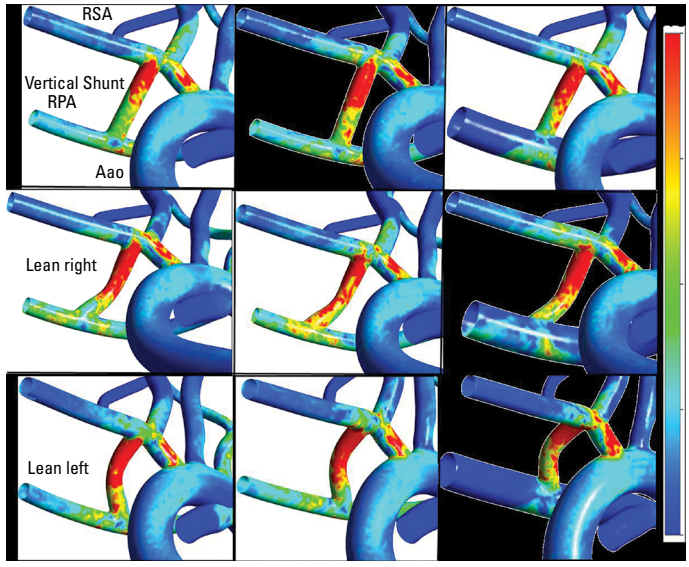

Figure 2. Close-up views of vessel wall shear stress distributions for all the shunt configurations studied. Red color indicates high wall shear stress regions due to blood flow.
Aao - aorta; RSA - right subclavian artery; RPA - right pulmonary artery; WSS - wall shear stress

After studying all of the configurations, it was seen that in the case of equal diameter arteries, vertical shunt configuration produced the lowest total flow rate. There was no statistically significant difference in LPA and total pulmonary flow rates ($p>0.05$), whereas there was a significant difference in RPA pulmonary flow rates ($p=0.032$) according to the shunt angle (Table 3). Binary evaluations using the Bonferroni–Dunn post-hoc test revealed that measurements with vertical configuration had larger pulmonary flow rate values than those with lean left configuration ($p=0.026$). There was no statistically significant difference in RPA, LPA, and total pulmonary flow rates according to the diameter ($p>0.05$) (Table 4).

Taken together, as far as this idealized model is concerned, these data suggest that the mBT shunt conduit should not be leaned toward the narrow PA to achieve the best flow rates. Our

Table 3. Comparison of pulmonary flow rates between angle configurations

		Vertical	Lean right	Lean left	*P*
RPA (n=3)	Median (Q1, Q3)	173 (172, 182)	171 (166, 172)	156 (151, 162)	0.032*
	Mean±SD	175.67±5.51	169.67±3.21	156.33±5.51	
LPA (n=3)	Median (Q1, Q3)	146 (122, 165)	132 (127, 142)	149 (141, 168)	0.329
	Mean±SD	144.33±21.55	133.67±7.64	152.67±13.87	
Total (n=3)	Median (Q1, Q3)	329 (295, 337)	298 (298, 314)	305 (303, 319)	0.558
	Mean±SD	320.33±22.30	303.33±9.24	309.00±8.72	

Kruskal–Wallis test (Q1 - first quartile; Q3 - third quartile; SD - standard deviation)
*$P<0.05$

Table 4. Comparison of pulmonary flow rates between diameter configurations

		R=4 mm&L=4 mm Median (Q1, Q3)	R=4 mm&L=8 mm Median (Q1, Q3)	R=8 mm&L=4 mm Median (Q1, Q3)	*P*
RPA (n=3)	Median (Q1, Q3)	171 (156, 173)	166 (151, 172)	172 (162, 182)	0.578
	Mean±SD	166.67±9.29	163.00±10.82	172.00±10.00	
LPA (n=3)	Median (Q1, Q3)	127 (122, 149)	165 (132, 168)	142 (141, 146)	0.329
	Mean±SD	132.67±14.36	155.00±19.97	143.00±2.65	
Total (n=3)	Median (Q1, Q3)	298 (295, 305)	319 (298, 337)	314 (303, 329)	0.241
	Mean±SD	299.33±5.13	318.00±19.52	315.33±13.05	

Kruskal-Wallis test (Q1 - first quartile; Q3 - third quartile; SD - standard deviation)

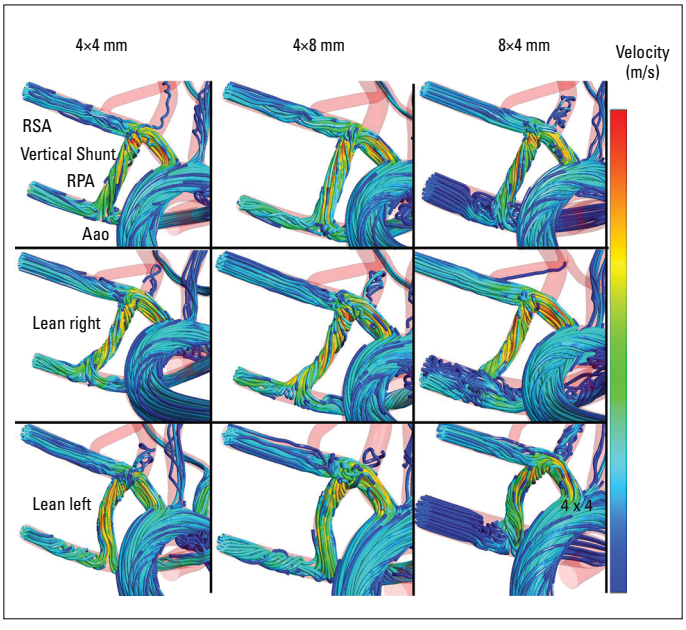

Figure 3. Close-up views of velocity streamlines for all the shunt configurations studied

model employed equal PVR for both lungs to illustrate the effect of great vessel diameter. The hemodynamic effects of unbalanced PVR may be more severe than the diameter effects and require further simulations.

Energy loss

The calculated energy losses for all cases are shown in Table 5. There was no statistically significant difference in energy loss between diameter combinations (p=0.430) and angle combinations (p=0.193).

When the shunt flow was directed to the PAs through an artificial shunt increased the energy loss has increased. For all cases, the energy losses were ~400%±5%. Much more improved cases in terms of energy efficiency can be achieved; however, they are not preferable since they do not produce enough output for PA feeding, even though they are more energy efficient.

Wall shear stress

Wall shear stress (WSS) tends to be higher around shunts, particularly at the anastomosis region of the systemic arteries and shunt (Fig. 3). The anastomosis region of the shunt and PA also has relatively higher WSS zones. A very low or sharp WSS change may cause plaque formation inside the vessel and/or shunt (10-13). As the flow inside the shunt increased, WSS tended to increase due to the increased velocity gradients.

Effect of pulmonary resistance

Table 6 shows the pulmonary flow rates of RPA, LPA, and total PA for lower and higher pulmonary resistance values compared with the baseline case (configuration 1). There was no statisti-

Anatol J Cardiol 2018; 20: 2-8
DOI:10.14744/AnatolJCardiol.2018.54810

Table 5. Comparison of calculated energy loss (10^{-3} kg m^2/s^3) between angle and diameter configurations

	4×4 mm	4×8 mm	8×4 mm	Median (Q1, Q3)	Mean±SD	*P*
Vertical (90°)	414	389	369	389 (369, 414)	390.67±22.55	
Lean right (60°)	407	433	415	415 (407, 433)	418.33±13.32	0.430
Lean left (60°)	431	419	404	419 (404, 431)	418.00±13.53	
Median (Q1, Q3)	414 (407, 431)	419 (389, 433)	404 (369, 415)			
Mean±SD	417.33±12.34	413.67±22.48	396.00±24.02			
P	**0.193**					

Kruskal-Wallis test (Q1 - First quartile; Q3 - Third quartile; SD - standard deviation)

Table 6. Comparison of pulmonary flow rates (10^{-4} kg/s) for RPA-LPA in cases with different resistance values with respect to baseline (conf. 1)

	RPA	LPA	Total
Baseline (conf. 1) (n=1)	173	123	296
RPA R: 100% LPA R: 80% (n=1)	173	140	313
RPA R: 80% LPA R: 100% (n=1)	183	124	307
RPA R: 80% LPA R: 80% (n=1)	191	136	327
RPA R: 120% LPA R: 100% (n=1)	175	131	306
RPA R: 100% LPA R: 120% (n=1)	180	126	306
RPA R: 120% LPA R: 120% (n=1)	164	131	295
P	**0.423**	**0.423**	**0.423**

Kruskal-Wallis test; RPA - right pulmonary artery; LPA - left pulmonary artery; conf. - configuration; R - resistance value

cally significant difference in RPA, LPA, or total pulmonary flow rate among the seven configurations (all p=0.423). As expected, an increase in resistance causes a decrease in the pulmonary flow and vice versa. Since the resistance change was limited by 20% change, the flow rate change was also limited (around 10%).

Blood damage

Shear strain formed by blood flow may cause damage to the red blood cells. Total blood damage throughout the shunt and pulmonary arteries are presented in Table 7. The results show that there was no statistically significant difference in the blood damage values between the diameter combinations (p=0.733). In addition, there was no statistically significant difference in the blood damage values between the angle combinations (p=0.252).

Statistical analysis

Number Cruncher Statistical System 2007 (NCSS; Kaysville, Utah, USA) program was used for statistical analysis. Descriptive statistical methods (median, first-quarter, and third-quarter) were used when the study data were evaluated. Normal distributions of quantitative data were tested with the Shapiro–Wilk and graphical tests. The Kruskal–Wallis test and Bonferroni–Dunn post-hoc test were used for two-way intergroup comparisons of quantitative variables with no normal distribution. Statistical significance was accepted as $p<0.05$. Uncertainly in CFD simulations obtained from mesh sensitivity analysis is based on this statistical analysis.

Discussion

mBTS is the key palliative procedure in patients undergoing congenital heart surgery. However, it is still associated with high morbidity and mortality in both infants and neonates because of shunt occlusion, shunt failure, or excessive pulmonary blood flow. In the majority of neonates, most stages of cardiac repair are performed between 3 months and 2 years after the primary shunting stage, depending on the primary diagnosis and procedure performed. Although progress has been made in primary total correction and the perioperative management of neonates and children with congenital heart diseases, palliative procedures still play a vital role in high-risk patients with complex cardiac lesions such as hypoplastic left heart syndrome (14).

mBTS are performed in patients with complex heart defects involving restricted PA flow. The size of the employed polytetrafluoroethylene graft strictly depends on the patient's age and body weight and the PA branch size. A small-diameter mBTS graft and narrow PA coexisting with increased pulmonary tension or polycythemia are significant risk factors for shunt occlusion (15). Shunt occlusion may occur suddenly, resulting in abrupt deterioration of the patient's condition or death. At times, the graft occlusion process is gradual and causes a slow increase in hypoxia, cyanosis, and impaired exercise tolerance. The usual cause of shunt occlusion is acute thrombus closing the narrow lumen of the graft, which in most cases is narrowed further by coexisting distal stenosis at the junction of the mBTS graft and narrow PA branch. Successful early recanalization of a graft is possible with the use of combined local or systemic thrombolytic therapy and successful balloon angioplasty (5). However, this type of treatment is usually ineffective in patients with gradually developing occlusions because the mechanics of narrowing or closing are quite different, focal neointimal hypertrophy as well

Table 7. Comparison of calculated blood damage (dimensionless) values between angle and diameter configurations

	4×4 mm	4×8 mm	8×4 mm	Median (Q1, Q3)×10^{-3}	Mean±SD×10^{-3}	*P*
Vertical (90°)	2.11×10^{-3}	3.80×10^{-3}	2.06×10^{-3}	2.11 (2.06, 3.80)	2.66±0.99	
Lean right (60°)	3.79×10^{-3}	3.64×10^{-3}	2.29×10^{-3}	3.64 (2.29, 3.79)	3.24±0.83	**0.733**
Lean left (60°)	5.85×10^{-3}	3.11×10^{-3}	4.42×10^{-3}	4.42 (3.11, 5.85)	4.46±1.37	
Median (Q1, Q3)×10^{-3}	3.79 (2.11, 5.85)	3.64 (3.11, 3.80)	2.29 (2.06, 4.42)			
Mean±SD×10^{-3}	3.92±1.87	3.52±0.36	2.92±1.30			
P	**0.252**					

as calcifications and mural thrombus in the shunt lumen causes shunt occlusion. In these cases, effective graft recanalization is possible if it follows endovascular stent implantation, which can stabilize hypertrophic neointima in the graft lumen (5).

There is a strong relationship between WSS distribution versus plaque formation and endothelial vessel layer damage (10). Low WSS causes blood damage via thrombosis formation, whereas high WSS may corrode endothelial cells. In particular, the anastomosis regions between the subclavian artery and conduit have a higher WSS in most configurations, whereas anastomosis regions between the conduit and PA have lower WSS distributions. Therefore, as the present results indicated, conduit corrosion may start in the upper regions, but obstructions may begin to form in the lower regions of the conduit and RPA anastomosis regions. Furthermore, since vertical shunt configurations have higher WSS distributions with respect to leaned shunt configurations, vertical shunt cases are not vulnerable to platelet activation and thus to thrombosis formation in the short term after surgery.

Blood damage quantification through shear strain rate is another quantification technique of blood and vessel malformation. Our findings have shown that the configuration might cause 100% difference in the amount of total blood damage (Table 5). This is a substantial difference and should be predicted during surgery planning. Another important finding was that the narrower pulmonary arteries and leaned anastomosis configurations tended to have higher blood damage than larger arteries and vertical configurations, respectively.

The configurations generated by resistance changes show that the pulmonary resistance regulations, besides shunt anastomosis angle and PA size, may be an alternative for controlling the flow rate. A 20% decrease in the resistance value can cause a flow rate increase equal to a 100% diameter enlargement.

Although mBTS has improved the care of patients undergoing treatment for congenital heart diseases, controlling the blood flow through the conduit remains challenging. Although Doppler was used to predict pulmonary blood flow (16), more recent studies have used computational imaging to measure blood flow in individual patients. For example, Liu et al. (17) used CFD, echocardiography, and pulsatile pressure waves to study real-time velocity after mBTS, blood flow distribution, local pressure, and WSS. The authors concluded that the pressure decreases through the conduit and that the combination of WSS and pulsatile pressure can lead to blood cell damage. These studies are crucial for evaluating the outcome of mBTS and optimizing future implants.

The present results provide a look-up table based on PA sizes to guide clinicians in their decision-making prior to surgery. Due to the complexity of the problem, there are several limitations that are often inevitable during cardiovascular modeling. This parametric study has been achieved using computational cardiovascular models which have been validated in a previous study for fixed patient anatomy and cardiac output (7). It was necessary to perform a parametric study and clarify the possible effects of shunt configuration and PA sizes. These parameters have a certain patient-to-patient variation, which can influence the results accordingly. Many such patients do not have a lot of physical space for realization of configurations that are theoretically possible. In reality, there is often not much space between PDA insertion and PA branch division in the hilum of the lung. To achieve a 60° angulation beveling might not be sufficient and the mBTS itself would have to be longer than the standart straight. Also, the PA sizes might change substantially for different patients. Still, the present calculations illustrate surgically significant trends for an ideal patient, providing expected mean hemodynamic values. The next step of the current study is to plan clinical trials and assessment methodology of the surgery performance based on the proposed parametric configurations. Other than clinical restrictions, there are several modeling limitations: rigid artery wall assumption, Newtonian blood flow, and steady flow dynamics. These assumptions can be justified by the fact that the present study compared the results within each configuration. Furthermore, the steady-state simulations are accepted as accurate for predicting the flow splits at the outlets of the arteries since the inlet boundary condition represents the time-averaged (mean) flow conditions (18, 19). Since we used large arteries as models, the blood flow was relatively Newtonian. Compliant wall conditions can increase the accuracy of the model, but accurate material parameters are needed and this is out of the scope of the current study.

Anatol J Cardiol 2018; 20: 2-8
DOI:10.14744/AnatolJCardiol.2018.54810

Conclusion

The current study demonstrated that the anastomosis angle between the conduit and PA has a crucial effect on the flow splits directed to PA. In addition, the WSS distribution changes substantially with respect to those two parameters. Due to total pulmonary flow rates decrease, the shunt angle should not be directed toward the narrow PAs. Vertical anastomosis configurations increase the total PA flow; thus, these configurations are preferable compared with leaned anastomosis conduit configurations. Furthermore, the pulmonary resistance can be another factor controlling the pulmonary flow rates.

Acknowledgement: Funding was provided by Grants from the European Research Council (ERC) Proof of Concept Grant KidsSurgicalPlan, ERC Starting Grant 307460, TUBITAK 1003 priority-research program Grant 115E690 and TUBITAK award 2219–1059B191501944.

Conflict of interest: None declared.

Peer-review: Externally peer-reviewed.

Authorship contributions: Concept – A.A., Y.Y., T.S.; Design – A.A., T.S.; Supervision – A.A., Y.Y., K.P.; Materials – A.A., Ş.P., G.N.O.; Data collection &/or processing – Ş.P., G.N.O., K.P.; Analysis &/or interpretation – Ş.P., G.N.O., K.P.; Literature search – A.A., Ş.P.; Writing – A.A., Ş.P., G.N.O.; Critical review – A.A., Ş.P., Y.Y., K.P.

References

1. Erek E, Yalçınbaş YK, Mamur Y, Salihoğlu E, Turan T, Çolakoğlu A, et al. Systemic-to-pulmonary shunt operation in neonates with ductus-dependent pulmonary blood flow. Turkish J Thorac Cardiovasc Surg 2007; 15: 29-35.
2. Blalock A, Taussig H. The surgical treatment of malformations of the heart: in which there is pulmonary stenosis or pulmonary atresia. JAMA 1945; 128: 189-202. [CrossRef]
3. de Leval MR, McKay R, Jones M, Stark J, Macartney FJ. Modified Blalock-Taussig shunt. Use of subclavian artery orifice as flow regulator in prosthetic systemic-pulmonary artery shunts. J Thorac Cardiovasc Surg 1981; 81: 112-9.
4. Myers JW, Ghanayem NS, Cao Y, Simpson P, Trapp K, Mitchell ME, et al. Outcomes of systemic to pulmonary artery shunts in patients weighing less than 3 kg: Analysis of shunt type, size, and surgical approach. J Thorac Cardiovasc Surg 2014; 147: 672-7. [CrossRef]
5. Moszura T, Zubrzycka M, Michalak KW, Rewers B, Dryzek P, Moll JJ, et al. Acute and late obstruction of a modified Blalock-Taussig shunt: a two-center experience in different catheter-based methods of treatment. Interact Cardiovasc Thorac Surg 2010; 10: 727-31.
6. Dur O, Coskun ST, Coskun KO, Frakes D, Kara LB, Pekkan K. Computer-Aided Patient-Specific Coronary Artery Graft Design Improvements Using CFD Coupled Shape Optimizer. Cardiovasc Eng Technol 2011; 2: 35-47. [CrossRef]
7. de Zélicourt D, Jung P, Horner M, Pekkan K, Kanter KR, Yoganathan AP. Cannulation strategy for aortic arch reconstruction using deep hypothermic circulatory arrest. Ann Thorac Surg 2012; 94: 614-20.
8. Piskin S, Ündar A, Pekkan K. Computational Modeling of Neonatal Cardiopulmonary Bypass Hemodynamics With Full Circle of Willis Anatomy. Artif Organs 2015; 39: E164-75. [CrossRef]
9. Arora D, Behr M, Pasquali M. A tensor-based measure for estimating blood damage. Artif Organs 2004; 28: 1002-15. [CrossRef]
10. Tanweer O, Wilson TA, Metaxa E, Riina HA, Meng H. A comparative review of the hemodynamics and pathogenesis of cerebral and abdominal aortic aneurysms: lessons to learn from each other. J Cerebrovasc Endovasc Neurosurg 2014; 16: 335-49. [CrossRef]
11. Cunningham KS, Gotlieb AI. The role of shear stress in the pathogenesis of atherosclerosis. Lab Invest 2005; 85: 9-23. [CrossRef]
12. Peiffer V, Sherwin SJ, Weinberg PD. Does low and oscillatory wall shear stress correlate spatially with early atherosclerosis? A systematic review. Cardiovasc Res 2013; 99: 242-50. [CrossRef]
13. Fitts MK, Pike DB, Anderson K, Shiu YT. Hemodynamic Shear Stress and Endothelial Dysfunction in Hemodialysis Access. Open Urol Nephrol J 2014; 7(Suppl 1 M5): 33-44.
14. Shibata M, Itatani K, Oka N, Yoshii T, Nakamura Y, Kitamura T, et al. Optimal Graft Size of Modified Blalock-Taussig Shunt for Biventricular Circulation in Neonates and Small Infants. Int Heart J 2015; 56: 533-6. [CrossRef]
15. Gedicke M, Morgan G, Parry A, Martin R, Tulloh R. Risk factors for acute shunt blockage in children after modified Blalock-Taussig shunt operations. Heart Vessels 2010; 25: 405-9. [CrossRef]
16. Chaudhari M, Balmer C, Heng JT, Wright J, Stümper O. Usefulness of Blalock-Taussig shunt Doppler flow velocity profiles in the assessment of pulmonary artery pressure and flow. Eur J Echocardiogr 2004; 5: 111-7. [CrossRef]
17. Liu J, Sun QI, Hong H, Sun Y, Liu J, Qian Y, et al. Medical image-based hemodynamic analysis for modified Blalock-Taussig shunt. J Mech Med Biol 2015; 15: 1-17. [CrossRef]
18. Piskin S, Unal G, Arnaz A, Sarioglu T, Pekkan K. Tetralogy of Fallot Surgical Repair: Shunt Configurations, Ductus Arteriosus and the Circle of Willis. Cardiovasc Eng Technol 2017; 8: 107-19. [CrossRef]
19. Kheyfets VO, Rios L, Smith T, Schroeder T, Mueller J, Murali S, et al. Patient-specific computational modeling of blood flow in the pulmonary arterial circulation. Comput Methods Programs Biomed 2015; 120: 88-101. [CrossRef]